NJC

PAPER

View Article Online
View Journal | View Issue

Cite this: *New J. Chem.*, 2019, **43**, 18713

Fluorescence solvatochromism and modulated anticholinergic activity of novel coumarin compounds sequestered in human serum albumin nanocavities†

Mostofa Ataur Rohman, ‡ Prayasee Baruah,‡ Deboshika Bhattacharjee, B. Myrboh and Sivaprasad Mitra *

Received 25th June 2019,
Accepted 1st November 2019

DOI: 10.1039/c9nj03293b

rsc.li/njc

A coumarin compound, 3,3′-methylenebis(4-hydroxy-2*H*-chromen-2-one) (MHC), and its substituted derivative, 3,3′-(phenylmethylene)bis(4-hydroxy-2*H*-chromen-2-one) (MHCB), possess potent anticholinergic activities, which were found to be reduced significantly in the presence of human serum albumin (HSA). The molecular interactions responsible for sequestering MHC and MHCB were explored by steady-state and time-resolved fluorescence using the modulated solvatochromic behavior of the probes as a fluorescent marker. A quantitative description of the different solvent parameters responsible for the notable solvent-dependent photo-physical properties of the investigated systems was extracted from multiple linear regression analysis of the experimental data using the Kamlet–Taft and Catalán formalisms. A series of complimentary studies involving circular dichroism measurement and molecular docking calculations revealed that the binding of both coumarin derivatives resulted in the stabilization of the α-helical structure of human serum albumin (HSA). However, significant differences in binding mechanism were noted in terms of the strength, mode and principal forces responsible for the spontaneous association of the probes into the protein-binding domain.

Introduction

Coumarins, which are fragment organic compounds from the benzopyrone class, are naturally found in many plants and widely used in certain perfumes and fabric conditioners.[1–3] Since their first isolation in 1820, the coumarin group of compounds have been extensively studied due to their industrial, pharmaceutical, antimicrobial, antioxidant and anticancer properties.[4–10] The improved pharmacokinetic behaviour in coumarins is believed to be due to their rapid absorption and metabolism in the body.[11] Further, coumarins have also been identified as active therapeutic agents having anticoagulant activity,[12] immuno-stimulatory properties for treating chronic infections,[13] anti-inflammatory property,[12] and potent edema protective functions.[14]

Fluorescent coumarins are also popular as dye materials[15] and in sensory applications to detect several metal cations.[16,17] Reports are also available to justify their use as efficient dopant candidates for the generation of organic light-emitting diodes (OLEDs).[18] In addition, this group of compounds shows a very high fluorescence quantum yield. Hence, they behave as promising fluorescent tags for probing a series of different complex chemical as well as biological media because of their strong polarity-dependent Stokes shift and substantial change in dipole moment on excitation.[19–21] Studies on the interaction of bioactive compounds with biologically relevant macromolecules are important in the scientific and medical fields since they provide the basic foundation for their application in the pharmaceutical sciences.[22,23] In a recent report, the development of a series of multispectral methods to exploit the interaction of HSA with two coumarin derivatives, 3-(furan-2-yl)-6-methyl-2*H*-chromen-2-one (FM) and 6-chloro-3-(furan-2-yl)-2*H*-chromen-2-one (CM), was presented.[24]

Recently, a substituted coumarin derivative, namely 3,3′-methylenebis(4-hydroxy-2*H*-chromen-2-one) (MHC) was reported as potential inhibitor for acetylcholinesterase (AChE).[25] In fact, enzymatic hydrolysis data revealed that the AChE inhibition property of MHC is comparable even with the FDA approved cholinergic drug donepezil, opening up the possibility of its use as potential drug for the treatment of Alzheimer's Disease (AD). However, the effectiveness of pharmacologically screened drug molecules is strongly dependent on their lipophilicity and/or hydrogen bond (HB) formation ability. Further, molecular docking

Centre for Advanced Studies in Chemistry, North-Eastern Hill University, Shillong 793 022, India. E-mail: smitra@nehu.ac.in, smitranehu@gmail.com

† Electronic supplementary information (ESI) available: Detailed protocol for the estimation of anticholinergic activity (ST1), Tables S1–S6 and Fig. S1–S5. See DOI: 10.1039/c9nj03293b

‡ Equal contributors to the work.

calculations revealed the importance of hydrogen bond formation in the binding process of MHC in the peripheral anionic site (PAS) of AChE. Therefore, it is imperative to analyse the nature of the solute–solvent interaction quantitatively in MHC, which has been screened as a potential AChE inhibitor (AChEI).

The solvent-dependent fluorescence behaviour of differently substituted coumarin derivatives has also attracted significant attention recently since different spectroscopic parameters such as position of the fluorescence maximum, fluorescence yield and the excited-state lifetime of the investigated coumarin compounds are found to be strongly dependent on the polarity and hydrogen bonding ability of the solvent and also on the nature and position of substitution in the parent coumarin scaffold. Therefore, understanding the solvent-dependent photophysical behaviour of coumarin derivatives and identifying the quantitative contribution of microscopic solvent properties are still an active area of research.

The nature of different types of interactions results in a marked change in the excited state in comparison with the ground state, specifically due to the extensive electron density redistribution upon excitation.[26] Normally, the description of the non-specific interaction of organic solutes with solvent involves polarity and/or polarizability. The extent of interaction depends on the solvent dielectric constant (ε), refractive index (n) and the dipole moment (μ) of the solute in its Franck–Condon (FC) and/or relaxed fluorescent (RF) states. The corresponding spectral indicator such as absorption (ν_{abs}) or fluorescence (ν_{fluo}) maximum (in wavenumber) of the solute varies linearly with solvent polarity function, which is the orientation polarizability (Δf) according to the Lippert–Mataga relation.[27,28]

A deviation in the observable spectroscopic behaviour from the traditional equations for the non-specific interactions mentioned above often indicates the presence of specific interactions of the solute with the solvent, mostly arising due to the formation of hydrogen bonds (HB) between the solute and the solvent. Solvatochromic studies quantifying the specific solute–solvent interaction were considered by employing $E_T(30)$, a uni-parametric scale developed by Dimroth and Reichard,[29] which represents the HB donation acidity (α) of protic solvents. A more general multi-parametric linear solvation energy relationship (LSER), formalized first by Kamlet, Taft and coworkers[30] and further developed by Catalán,[31] includes both α and solvent HB acceptance basicity (β). A series of recent literature reported both treatments to quantify the solute–solvent interaction for many organic heterocycles.[32–35]

In the present investigation, the anticholinergic activity of 3,3′-(phenylmethylene)bis(4-hydroxy-2*H*-chromen-2-one) (MHCB) is estimated and compared with that of MHC (structure shown in Scheme 1) described earlier.[25] A comprehensive description of the photophysical and fluorescence spectral behaviour of both compounds is presented in a series of different solvents both in terms of the KT and Catalán models. Interestingly, MHCB possess very close structural resemblance with warfarin, one of the most extensively studied fluorescent biomarkers for serum albumin proteins. Also, the AChE inhibitory efficiency of the investigated coumarins was shown to decrease significantly in serum albumin matrix, which signifies the strong sequestering tendency of human serum albumin (HSA). Therefore, the results on the spectral modulation and nature of the molecular interaction of both systems are also presented in the presence of a series of heterogeneous media such as cyclodextrin and HSA.

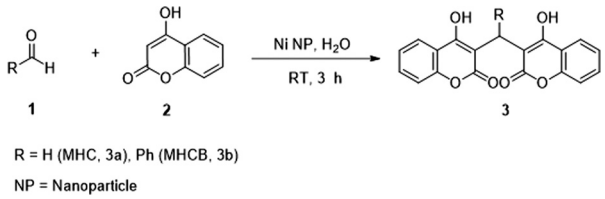

Scheme 1 Synthetic route and structural representation of the coumarin compounds investigated in the present study.

Results and discussion

Estimation of anticholinergic activity and its modulation in HSA

The kinetic parameters for the normal and inhibited enzyme hydrolysis pathways in the presence of the investigated coumarin compounds were obtained *via* the Michaelis–Menten (MM) analysis based on Scheme 2. Both coumarin compounds were found to inhibit acetylcholinesterase (AChE) activity in a non-competitive manner as apparent from the MM analysis. The comparative kinetic data of AChE inhibition and its modulation in the presence of HSA for both systems is shown in Fig. 1. The MM constant (K_m) remained practically unchanged, whereas, a notable alteration was seen in the V_{max} value. Also, the values of α and α' were found to be equal (where $\alpha = 1 + ([EI])/([E])$ and $\alpha' = 1 + ([IES])/([ES])$, respectively) since the inhibitor has equal probabilities of binding to the enzyme (E) and the enzyme–substrate (ES) complex (see ST1 in ESI†). In the case of non-competitive inhibition, inhibitors have been found to attach to the peripheral anionic site (PAS) of AChE, thereby posing no interference to the substrate binding catalytic anionic site (CAS).[36] The estimated IC_{50} values (Table 1) obtained from the modified Hill equation justifies both investigated coumarins as potent AChEIs, which have bright promise for possible utilization as a therapeutic avenue towards Alzheimer's disease (AD). The greater AChE inhibition potency for MHC and MHCB in

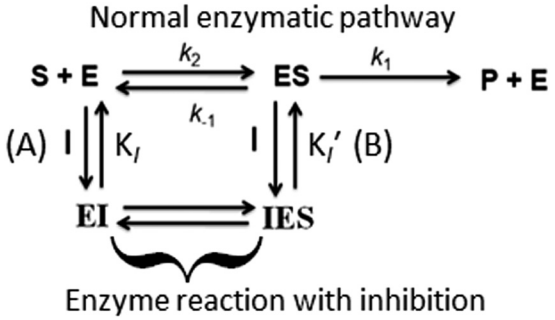

Scheme 2 Mechanistic representation of the normal and inhibited enzymatic activity of AChE. The competitive and uncompetitive inhibition paths are represented by (A) and (B), respectively, while the non-competitive inhibition involves both the pathways. The rate constants and the dissociation constants of individual steps are represented by *k* and *K*, respectively.

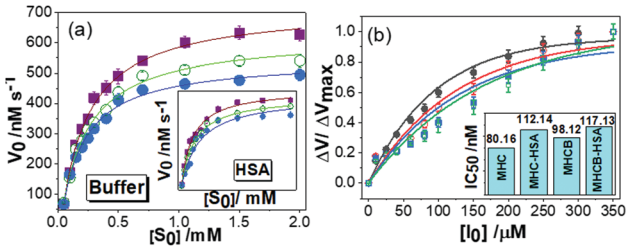

Fig. 1 (a) Hydrolysis curve (scattered points) for AChE activity (solid squares) and its inhibition in the presence of 5 nM (open circle) or 10 nM (solid circle) of MHCB in phosphate buffer solution of pH = 8.0. Inset shows the same experiment in HSA matrix. The solid line represents non-linear regression of the experimental data in each case. [AChE] = 0.079 U mL^{-1}. (b) Modified Hill analysis of AChE inhibition by MHC (circle) and MHCB (square) in aqueous buffer (solid points) and in the presence of HSA (empty points). Inset shows the corresponding IC_{50} values.

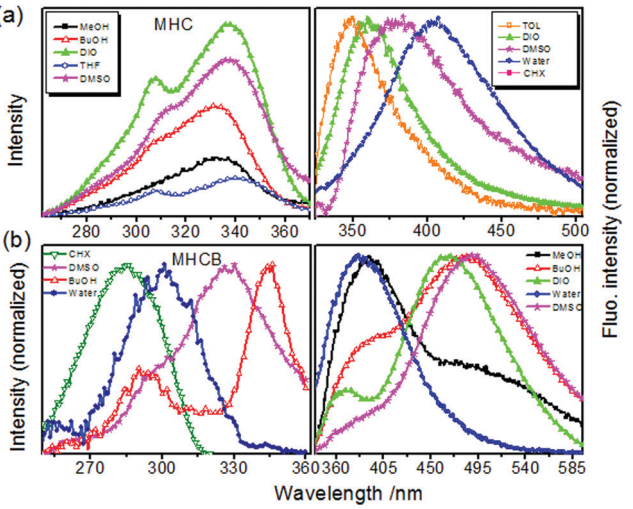

Fig. 2 Steady-state fluorescence excitation (left panel) and emission (right panel) spectra of MHC (a) and MHCB (b) in selected solvents. Solvent abbreviations: 1,4-dioxane (DIO), cyclohexane (CHX), toluene (TOL), tetrahydrofuran (THF), dimethyl sulfoxide (DMSO), acetonitrile (ACN), methyl alcohol (MeOH), and *n*-butanol (BuOH).

comparison with structurally similar chromone derivatives[37] is consistent with well-established structure activity relationship (SAR) reviews that the replacement of the coumarin skeleton with a chromone moiety results in the loss of AChE inhibition potency.[38]

Human serum albumin has been established as an effective bio-mimicking medium for AChE inhibition since the potencies of drugs have been found to be greatly modulated in the presence of HSA compared with aqueous buffer. Similarly, in the present investigation, HSA was found to decrease the inhibition potency of both MHC and MHCB considerably. For example, the estimated IC_{50} value in buffer medium for MHCB is 98.12 ± 7.9 compared to 80.16 ± 1.3 nM for MHC. However, in HSA matrix, this value changed to 117.13 and 112.14 nM, respectively. This shows that although in buffer medium the potency of MHC is higher, it is rendered almost equal for both compounds in HSA medium. Interestingly the relative change in IC_{50} value[39] was estimated to be 39% for MHC in comparison with only 20% for MHCB. These results indicate that the sequestering ability of HSA towards MHC is much stronger than that in the case of MHCB and in excellent agreement with the fluorescence titration results described later.

Steady-state spectral properties and solvent effect

The absorption profiles for both MHC and MHCB show a structured pattern and appear within the spectral range of 270–360 nm in all the solvents studied here (shown in ESI,† Fig. S1). On the other hand, the corresponding emission spectral peak appears in the range of 344–404 nm and 385–557 nm in different solvents for MHC and MHCB, respectively. The excitation spectra obtained by monitoring the fluorescence at the respective emission maximum presented unstructured profiles and appear within the corresponding absorption spectral range in both cases. The representative fluorescence emission and excitation spectral profiles for both MHC and MHCB in some selected solvents are shown in Fig. 2. Careful inspection of the emission spectral profiles reveals multi-dimensional solvent dependence for both systems. For example, the broad emission peak for MHC in water with a full width at half maximum (FWHM) of 5221 cm^{-1} shows the largest bathochromic shift (λ_{max} = 404 nm), while the corresponding spectrum in cyclohexane is extremely narrow (FWHM = 3987 cm^{-1}) and blue-shifted (λ_{max} = 350 nm). The emission peak maximum shows a continuous red shift with an increase in polarity of the medium. In contrast, for MHCB, the emission peak position in water and cyclohexane appears at 345 and 543 nm, respectively. There is no straightforward

Table 1 Kinetic data of AChE hydrolysis and the effect of different concentrations of MHCB as an inhibitor (I) on various parameters in aqueous buffer media and serum albumin matrix[a]

System	K_m/μM	V_{max}/nM s^{-1}	α	α′	IC_{50} (nM)	n_H
	From Michaelis–Menten equation				From modified Hill equation	
In buffer medium						
[I] = 0 nM	185 ± 20	817 ± 24	1.0	1.0	98.12 ± 7.9 (80.16 ± 7.1)	1.04 ± 0.08 (1.51 ± 0.1)
[I] = 5 nM	188 ± 23 (174 ± 24)	692 ± 21 (617 ± 24)	1.2	1.2		
[I] = 10 nM	166 ± 19 (166 ± 31)	623 ± 31 (527 ± 37)	1.3	1.3		
In HSA matrix						
[I] = 0 nM	178 ± 17	828 ± 23	1.0	1.0	117.21 ± 12.3 (110.34 ± 11.6)	1.10 ± 0.11 (1.51 ± 0.1)
[I] = 5 nM	190 ± 21 (178 ± 17)	730 ± 26 (667 ± 18)	1.1	1.1		
[I] = 10 nM	198 ± 19 (174 ± 22)	685 ± 39 (619 ± 22)	1.2	1.2		

[a] Corresponding data for MHC is given in parenthesis.[25]

Table 2 Various spectroscopic properties of the investigated chromone derivatives measured in a series of solvents[a]

Solvent	λ_{abs}/nm	ν_{abs}/cm^{-1}	λ_{em}/nm	ν_{em}/cm^{-1}	Stokes shift/cm^{-1}	$\phi_f/10^{-3}$	τ_{av}/ns	$\kappa_r/10^7$, s^{-1}	$\Sigma\kappa_{nr}/10^8$, s^{-1}
For MHC									
Cyclohexane	285	35 088	344	29 070	6018	15.42	8.76	0.20	1.12
Toluene	298	33 557	350	28 571	4986	2.29	9.13	0.03	1.09
1,4-Dioxane	301	33 223	360	27 778	5445	18.86	0.39	4.80	25.15
Acetonitrile	295	33 898	360	27 778	6121	2.00	2.34	0.09	4.25
Methanol	301	33 223	360	27 778	5445	0.85	2.44	0.03	4.10
Tetrahydrofuran	300	33 333	372	26 882	6452	0.76	0.64	0.10	15.61
DMSO	297	33 670	380	26 316	7354	9.00	1.34	0.70	7.42
Water	301	33 223	404	24 752	8470	68.00	0.84	8.10	11.09
Ethyl acetate	300	33 333	353	28 329	5005	3.02	0.51	0.60	19.50
n-Butanol	293	34 130	355	28 169	5961	6.44	2.65	0.20	3.70
For MHCB									
Cyclohexane	328	30 488	543	18 416	12 072	0.46	9.54	0.005	1.04
Toluene	326	30 675	557	17 953	12 722	0.31	7.69	0.004	1.29
1,4-Dioxane	338	29 586	466	21 459	8127	2.50	0.72	0.300	13.81
Acetonitrile	334	29 940	493	20 284	9656	0.42	0.51	0.083	19.72
Methanol	332	30 120	487	20 534	9587	0.27	1.34	0.020	7.43
Tetrahydrofuran	340	29 412	459	21 786	7625	0.53	1.19	0.044	8.37
DMSO	337	29 674	490	20 408	9265	2.30	0.57	0.400	17.53
Water	324	30 864	385	25 974	4890	1.00	0.47	0.200	21.40
Ethyl acetate	340	29 412	465	21 505	7906	1.70	0.91	0.200	10.95
n-Butanol	332	30 120	484	20 661	9459	1.30	0.62	0.200	16.18

[a] Corresponding solvent properties are listed in the ESI (Table S1).

correlation between emission maximum and solvent polarity in this case. However, the emission spectral profiles show a distinctive shape within these two extremes and the intensity ratio of these two peaks varies significantly in different solvents. The results indicate that despite their similar structural motif, the solvent response to the corresponding fluorescence states of MHC and MHCB is distinctly different. In addition to the absorption and emission peak position (λ_{abs} and λ_{em}, respectively), other spectral parameters such as Stokes shift ($\Delta\nu_{ss}$) and fluorescence yield (ϕ_f) are also listed in Table 2 for both systems.

Time-resolved fluorescence behaviour

Extensive fluorescence lifetime measurements were performed for both MHC and MHCB in different solvents by monitoring the fluorescence at their emission maximum. For both systems, the accepted fitting model and the magnitude of τ_{av} is strongly dependent on the nature of the solvent (Fig. S2, ESI†). For example, although the experimental traces can be adequately expressed by a single exponential decay function for MHCB in most of the solvents studied here (with a decay time in the range of 0.5–1.3 ns), a two-exponential model was necessary to reproduce the data in non-interacting solvents such as cyclohexane and/or toluene (Fig. 3). On the other hand, MHC gives a two-exponential decay in most of the solvents. However, a minimum of a three-exponential decay function is necessary to fit the data in cyclohexane and/or toluene with acceptable statistical parameters. The complete results for the fluorescence decay fitting along and statistical parameters for both compounds in different solvents are given in the ESI† (Table S2).

The calculated average lifetime (τ_{av}) values for all the systems are also presented in Table 1. Further, estimation of the radiative (κ_r) and total non-radiative ($\Sigma\kappa_{nr}$) decay rate constants in each case was performed using the known values of ϕ_f and τ_{av}. It was

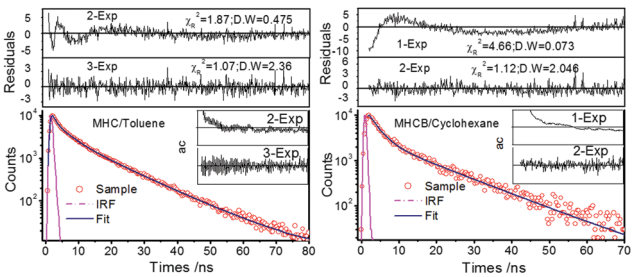

Fig. 3 Time-resolved fluorescence decay profile (open circles) and simulated data (solid line) of MHC in toluene (left) and MHCB in cyclohexane (right). IRF indicates the instrument response function. Visual inspection of the distribution of weighted residuals and autocorrelation function (ac) confirms the applicability of 3- and 2-exp decay model for simulation of experimental data in the respective cases.

observed that for all the systems, the magnitude of $\Sigma\kappa_{nr}$ is quite high and almost two orders of magnitude larger than the rate constants for the radiative processes (κ_r). Thus, the non-radiative decay process predominates in the deactivation of the excited state of both coumarins. Overall, the steady-state and time-resolved fluorescence data of the investigated coumarin compounds show significant solvent dependence. However, there is no straightforward correlation between this solvatochromism with a single physico-chemical property such as polarity and/or viscosity of the solvent. Therefore, it is believed that the interaction of these probes with solvent needs to be modeled by considering both the non-specific and specific interactions.

Fluorescence studies in mixed solvents

The importance of a specific solvent effect in controlling the excited-state photo-physical behaviour of the investigated compounds was

further justified by monitoring the fluorescence in a series of mixed solvents. The fluorescence property showed complex changes in different compositions of binary solvent mixtures comprising one or more of the following signatures: (i) momentous change in fluorescence intensity, (ii) shift in fluorescence spectral position, and (iii) notable difference in the width of the fluorescence spectrum. Some representative examples of MHC in dimethyl sulfoxide (DMSO)/water mixture is shown in Fig. 4(a), while the corresponding figures in DMSO/methanol and water/acetonitrile mixtures are given in the ESI† (Fig. S3). It is interesting to note that while the fluorescence intensity of MHC in DMSO underwent steady quenching with an increase in the mole fraction of methanol presumably due to the formation of solvent hydrogen bonding, the introduction of water in an acetonitrile solution resulted in an increase in intensity. Therefore, it is obvious that the specific interaction through hydrogen bond formation is not the only factor controlling the spectral intensity. Further, the width of the fluorescence spectrum underwent a significant increase in water compared with that in acetonitrile solution. On the other hand, the addition of water in the DMSO solution of MHC led to an increase in fluorescence intensity at a low water concentration until it reached a maximum and then further decreased at a higher water proportion (inset Fig. 4a). A gradual red shift in the fluorescence maximum was also noted during this process. However, this situation was far more complex and interesting for MHCB (Fig. 4b). The fluorescence emission maximum of MHCB in DMSO appeared at 485 nm. On increasing the mole fraction of water, the intensity of this band decreased with a concomitant increase in the intensity of a new peak at 385 nm (inset Fig. 4b). The presence of a clear iso-emissive point at 445 nm indicates the equilibrium between the two differently hydrogen bonded complexes of MHCB with DMSO and water, giving the emission spectral peak at 485 and 385 nm, respectively.

The fluorescence decays were collected using a fixed excitation wavelength (λ_{exc} = 295 nm) at the magic angle for both compounds in different mixed solvent compositions. The emission was monitored at the maximum wavelength of the corresponding spectrum in the case of MHC. However, time-resolved data was collected both at 385 and 485 nm at each solvent composition for MHCB. Some of the representative decay profiles are shown in Fig. 4c and in the ESI† (Fig. S3). The notable deviation in the decay profiles with the solvent composition confirms the significant solvent effect on the excited-state relaxation process in both compounds. The details of the fluorescence decay fitting and the corresponding average lifetimes (τ_{av}) are listed in the ESI† (Table S3). Interestingly, analogous to the fluorescence intensity variation pattern, the τ_{av} values of MHC also increased until the mole fraction of water reached *ca.* 0.85 and then it decreased monotonically. A similar pattern was also observed for the fluorescence lifetime of MHCB obtained by monitoring the emission at 485 nm. The rather unusual behaviour in the DMSO/water mixture with a high water content (with $x_{DMSO} \approx 0.15$) is quite well known[40,41] and consistent with the observation of an abrupt increase in solvent hydrophobicity under this condition estimated from molecular dynamics (MD) simulation.[42] The present results indicate that the fluorescing states representing the relaxation of MHC and MHCB at 485 nm are relatively nonpolar in nature. However, the MHCB fluorescence at 385 nm originates from a species that is significantly different in nature and mostly controlled by a specific solvent interaction. Overall, both the steady-state and time-resolved fluorescence studies in mixed solvents further reaffirm the multi-faceted mode of solvent action on the relaxation spectroscopic behaviour of the investigated coumarin compounds.

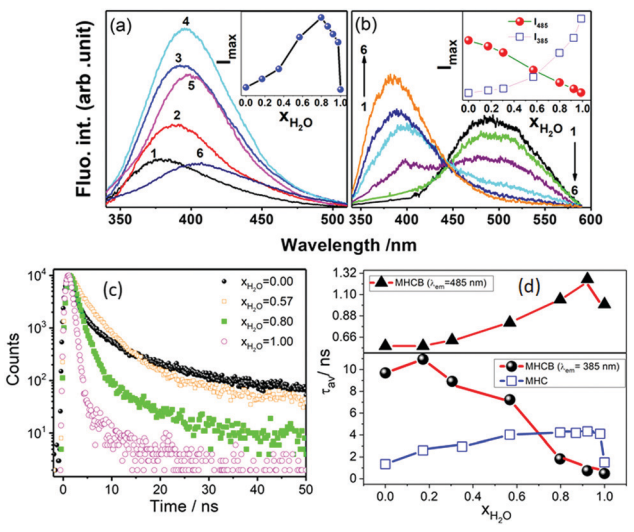

Fig. 4 Fluorescence emission spectra of MHC (a) and MHCB (b) in DMSO/water mixture with changing mole fraction (x) of water as 0 (1), 0.35 (2), 0.57 (3), 0.80 (4), 0.92 (5) and 1.00 (6). Inset shows the intensity variation of emission maximum in the respective case. (c) Time-resolved fluorescence decay traces obtained by monitoring MHCB fluorescence at 385 nm with a variation in water content in DMSO/water mixture. (d) Variation in average fluorescence decay time (τ_{av}) for MHC and MHCB with an increase in the mole fraction of water.

Quantitative estimation of the contribution from solvent parameters

The spectroscopic behaviour of the coumarin compounds depends strongly on the nature of the solvent. To describe this solvatochromism through quantitative estimation of different solvent parameters, all the quantities listed in Table 1 were subjected to multiple regression analysis based on the Kamlet–Taft (KT) and Catalán models. The analysis results are displayed in the ESI† (Tables S4 and S5, respectively, ESI†), and Fig. 5 shows the percentage contribution of each of these parameters towards different spectroscopic properties in a variety of solvents.

It should be noted that for both systems, specific solvent interactions characterized by solvent hydrogen bond donation acidity (α) and acceptance basicity (β) contribute strongly in addition to the solvent dipolarity/polarizability contribution (π^* parameter). For both MHC and MHCB, the qualitative contribution of the different solvent parameters towards the photophysical behaviour of the absorbing species (characterized by ν_{abs}^{max}) is almost equivalent. The only significant difference is the relatively higher contribution (*ca.* 50%) of the π^* parameter in MHC compared with the mere 15% in MHCB. However, in addition to the significant contribution of β (30–40%) in emission

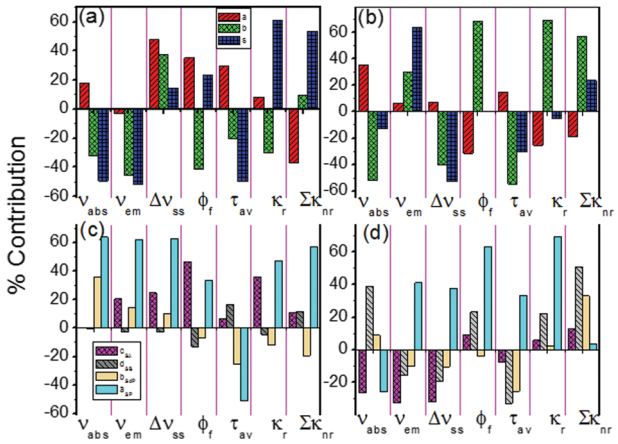

Fig. 5 Percentage contribution of solvent parameters obtained from the Kamlet–Taft (top panel) and Catalán (bottom panel) analysis for the different spectroscopic properties of MHC (a and c) and MHCB (b and d). The properties listed here are absorption and emission peak (ν_{abs} and ν_{em}, respectively), Stokes shift ($\Delta\nu_{ss}$), quantum yield (ϕ_f), average fluorescence lifetime (τ_{av}), radiative and total non-radiative rate constant (κ_r and $\Sigma\kappa_{nr}$).

spectral maximum (ν_{em}^{max}), the major contribution originates from the π* parameter (50–55%), even though it acts in exactly the opposite way for MHC and MHCB. For example, KT analysis predicts that the fluorescence maximum will shift towards a lower wavelength (increase in the value of ν_{em}^{max}) in highly polar solvents such as water for MHCB, whereas, it is exactly opposite in the case of MHC. These predictions correlate well with the fluorescence data of the investigated systems given in Fig. 2 and Table 2. Despite the similar structural motifs of MHC and MHCB, the striking difference in the solvent response towards their photophysical behaviour is intriguing. For example, while the variation in fluorescence yield (ϕ_f) constitutes *ca.* 20% contribution from the π* parameter in the case of MHC, it is almost insignificant for MHCB. Further, the contribution of the α and β parameters towards ϕ_f in these systems is contradictory. As discussed before, the non-radiative rate constant ($\Sigma\kappa_{nr}$) plays a dominant role in the excited-state deactivation process for both coumarins. Interestingly, all three solvent parameters contribute in the same direction towards the change in $\Sigma\kappa_{nr}$ for both systems, even though in a significantly different amount. It should be noted here that while the contribution from the solvent α and β parameters changes $\Sigma\kappa_{nr}$ in an analogous way for MHC and MHCB, the contribution of the π* term is almost two and half times more in the former.

Thus, the importance of the π* term, particularly in the regression analysis of the spectral behaviour of these coumarin derivatives needs further exploration. Unfortunately, quantitative separation of the solvent dipolarity and polarizability effect cannot be achieved in the KT formalism. However, the recent development of the Catalán four-parameter solvent scale separates these two quantities and gives more detailed information on the non-specific behaviour of the solvatochromic interaction. The results of the regression analysis of all the properties of MHC and MHCB using the Catalán solvent scale are also included in Fig. 5 (lower panel). It should be noted here that although the individual spectral properties give relatively better correlation with the Catalán formalism than the KT analysis, the qualitative results of the different solvatochromic behaviours are almost similar in both cases.

Fluorescence modulation in cyclodextrin nanocavities

Cyclodextrins (CDx) are extensively used as cyclic components for the construction of supramolecular architectures because of their well-defined ring structure and affinity for different classes of compounds of varying size and shape. The unique behaviour of CDx to encapsulate organic compounds inside their hydrophobic central cavity make them potential candidates as extremely efficient molecular vehicles for drug delivery.[43,44] Furthermore, binding of a fluorescent guest in the interior of the cavity of CDx renders an opportunity to study different photophysical properties in tailored environmental conditions. The results discussed in the previous sections indicate that the spectral features of both MHC and MHCB depend strongly on various solvent parameters, including hydrogen bonding ability. Therefore, it will be interesting to monitor the fluorescence of these compounds in the nanocavities of CDx.

The effect of β-CDx (consisting of a macrocyclic ring of seven glucose subunits joined by α-1,4 glycosidic bonds) on the spectral properties of the investigated systems was studied by keeping the concentration of the probe fixed and changing the concentration of the added β-CDx. The absorption spectra of none of these compounds showed notable changes upon the addition of cyclodextrin, except a minor increase in absorption intensity presumably due to the improved dissolution of the probes in the presence of β-CDx. However, the fluorescence spectra underwent drastic changes and interestingly, the spectral response of the investigated coumarin derivatives towards an increase in β-CDx concentration was distinctly different (Fig. 6). For example, the fluorescence intensity of MHCB increased with a significant red-shift in peak position from 396 nm to 420 nm in the presence of β-CDx. Typically, caging of a series of guest molecules in the β-CDx cavity led to an increase in fluorescence intensity due to the restricted motion of the encapsulated probe with reduced non-radiative decay pathways. Therefore, the effect of cyclodextrin on the intensity and position of the fluorescence spectrum in the case of MHCB seems compatible with the inclusion of the probe into the cavity. The binding constant (K) was estimated to be 132.40 ± 2.45 M^{-1} from the slope and intercept of linear variation in $1/(I - I_0)$ against 1/[β-CDx] (inset, Fig. 6b)

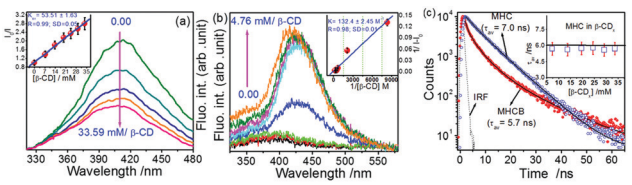

Fig. 6 Variation in fluorescence intensity (λ_{exc} = 305 nm) of MHC (a) and MHCB (b) with an increase in β-CDx concentration (along the arrow direction). Inset shows the corresponding SV and BH plots. (c) Time-resolved decay traces of MHC and MHCB (open and solid circles, respectively) together with the simulated data (solid line) with 2-exp decay function in the presence of 7.2 and 4.8 mM β-CDx, respectively. Inset: Variation in τ_{av} of MHCB with an increase in [β-CDx].

for 1:1 complex formation between β-CDx and MHCB using the Benesi–Hildebrand (BH) relation[45] given by eqn (1).

$$\frac{1}{I - I_0} = \frac{1}{I_\infty - I_0} + \frac{1}{K(I_\infty - I_0)} \times \frac{1}{[\mathrm{CD}]} \quad (1)$$

where I_0 and I_∞ are the fluorescence intensities of the free and fully complexed MHCB, respectively.

On the other hand, the fluorescence intensity of MHC decreased continuously in the β-CDx environment without any significant shift in peak position (Fig. 6a). It should be noted here that normally a fluorescent molecule experiences a relatively non-polar environment in an encapsulated complex in comparison with the bulk solution. It was already confirmed from the KT analysis (described in the previous section) that the fluorescence yield (ϕ_f) of MHC decreases with a reduction in polarity (given by π^* parameter), which is consistent with the present observation in the β-CDx environment. As confirmed from the time-resolved measurements (see below), the decrease in MHC fluorescence intensity in the presence of cyclodextrin is due to the ground state complex formation (static quenching). The association constant (K_a) under this situation can be approximated as the Stern–Volmer (SV) quenching constant (K_S) for static cases,[46] which is related with the fluorescence intensity and lifetime in the absence (given by I_0 and τ_0, respectively) and presence (I and τ, respectively) of a certain quencher concentration [Q] as:

$$\frac{I_0}{I} = 1 + K_S[\mathrm{Q}]; \quad \frac{\tau_0}{\tau} = 1 \quad (2)$$

The calculated value from the slope of the linear SV plot (inset, Fig. 6a) is 53.51 ± 1.63 M^{-1}, which indicates that the extent of interaction in this case is about two and half times less in magnitude compared with that of MHCB.

The time-resolved measurement in the β-CDx environment for both compounds showed a significant deviation from the single-exponential decay functions observed in aqueous environment. In addition to a similar time constant corresponding to the free (uncomplexed) fluorophore in the bulk aqueous phase, one extra component with a relatively longer decay time, presumably arising due to the formation of a host–guest complex, contributes about 30% of the total decay of MHC (Table S6, ESI†). Interestingly, the corresponding contribution from the encapsulated component is as high as 70% in the case of MHCB. This indicates that the propensity of complex formation with β-CDx in MHCB is relatively higher than that in MHC, which is further justified from the magnitude of the binding constants in the respective cases estimated from the steady-state experiments. Some of the representative decay traces are shown in Fig. 6c. It should be noted that while the magnitude of τ_{av} showed steady increase from 6.36 to 7.03 ns for MHCB with an increase in the β-CDx concentration from 1.4 to 4.8 mM (until saturation in steady state intensity was achieved), it remained practically insensitive at τ_{av} = 5.66 ± 0.06 ns in the case of MHC even at [β-CDx] = 33.6 mM (inset, Fig. 6c). The constant value of τ_{av} further reaffirms that the quenching of the MHC fluorescence with an increase in β-CDx concentration occurs through ground state complex formation.

Sequestration of the cholinergic drugs in human serum albumin matrix

The excited state photophysical behaviour of environment-sensitive fluorescence probes is known to be markedly affected in protein nanocavities. Further, the investigated systems were identified as potential anti-cholinergic candidates for the treatment of AD. However, the AChE inhibitory activity of these compounds including the Food and Drug Administration (FDA) approved AD drugs shows a significant diminution in the presence of serum albumin matrix.[25,39] Therefore, it is imperative to understand the nature of the interaction of these compounds with human serum albumin (HSA). In this section, we describe the fluorescence modulation and the nature of the binding interaction of the coumarin probes with HSA using a variety of spectroscopic techniques and molecular docking calculation.

Quenching of intrinsic HSA fluorescence in presence of MHC and MHCB

The absorption spectral maximum of HSA appears at 280 nm. Excitation at this wavelength resulted in a broad intrinsic protein fluorescence within the 290–450 nm range originating from aromatic residues such as tyrosine (tyr) and tryptophan (trp) moieties, with almost equal fluorescence yield.[46] The addition of both MHC and MHCB to the HSA solution resulted in a steady decrease in the protein fluorescence intensity (Fig. 7) due to the interaction of these coumarin probes with the aromatic residues in the protein binding domain (PBD). Equivalent results were also observed at other temperatures for both systems (Fig. S4 in the ESI†). Interestingly, the protein fluorescence spectral profile became broad with two distinctly visible emission maxima at *ca.* 305 and 335 nm with the addition of both MHC and MHCB. Although the spectral position of the first band remained practically unchanged and can be considered

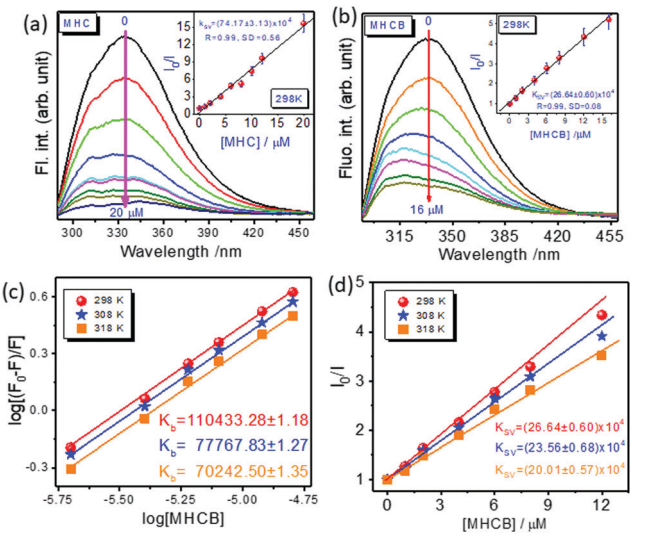

Fig. 7 Quenching of intrinsic HSA (1.2 μM) fluorescence in the presence of increasing MHC (a) and MHCB (b) concentration along the arrow direction. Inset shows the linear variation of the Stern–Volmer (SV) plot in each case. Temperature variation of binding constant (K_b) and SV constant (K_{SV}) values are shown for MHCB obtained from double-log (c) and SV (d) plots, respectively.

Table 3 Stern–Volmer quenching constant (K_{SV}), binding constant (K_b) and number of binding sites (n) calculated from the modulation of intrinsic protein (HSA) fluorescence data in the presence of varying MHC and MHCB concentration at different temperatures[a]

MHC						MHCB				
Temp./K	$K_{sv}/10^5$	$\log k_b$	n	ΔG	ΔH, ΔS	$K_{sv}/10^5$	$\log k_b$	n	ΔG	ΔH, ΔS
298	7.42 ± 0.31	7.26 ± 0.22	1.29 ± 0.04	−41.37	ΔH = 80.56,	2.66 ± 0.06	5.04 ± 0.07	0.92 ± 0.01	−28.30	ΔH = −10.94,
303	7.08 ± 0.31	7.04 ± 0.17	1.25 ± 0.03	−40.71	ΔS = −0.13	2.49 ± 0.07	4.94 ± 0.12	0.90 ± 0.02	−28.60	ΔS = 0.06
308	6.93 ± 0.30	6.83 ± 0.10	1.21 ± 0.02	−40.06		2.35 ± 0.06	4.89 ± 0.10	0.90 ± 0.01	−28.89	
313	6.50 ± 0.26	6.39 ± 0.13	1.13 ± 0.02	−39.40		2.24 ± 0.05	4.95 ± 0.09	0.92 ± 0.02	−29.18	
318	6.60 ± 0.34	6.48 ± 0.16	1.14 ± 0.03	−38.74		2.00 ± 0.07	4.85 ± 0.13	0.90 ± 0.03	−29.47	

[a] The mean values (±standard deviation) were estimated from three independent set of measurements; K_{SV} (M^{-1}) values are obtained from straight line fitting of protein Trp fluorescence quenching data using eqn (3), whereas $\log K_b$ and n values were obtained from double log plot (eqn (4)); the values of ΔH (kJ mol^{-1}) and ΔS (kJ mol^{-1} K^{-1}) obtained from the van't Hoff Plot (eqn (5)) were used to calculate ΔG (kJ mol^{-1}); and correlation coefficient (R^2) of straight line fitting is ≥0.98 in each case.

to originate from the tyrosinate moiety, the emission position at 335 nm (due to the tryptophan residue) showed a certain shift. The results indicate that with addition of the coumarin derivatives, there is a notable change in the protein secondary structure (see later) which results in varying degrees of exposure of the trp residue to the bulk aqueous phase. The Stern–Volmer (SV) relation for the protein fluorescence quenching data can be written in the form of eqn (3) at different temperatures.

$$\frac{I_0}{I} = 1 + K_{SV}[Q] = 1 + k_q\tau_0[Q] \quad (3)$$

where I_0 and I are the fluorescence intensities at 335 nm before and after the addition of the quencher (MHC or MHCB), respectively, k_q is the bimolecular quenching constant, τ_0 is the fluorescence lifetime of HSA in the absence of any quencher, and [Q] is the concentration of the quencher. The values of SV constant (K_{SV}) calculated from the slope of the linear SV plots and listed in Table 3 are 7.42 ± 0.31 and 2.66 ± 0.06 (10^5, M^{-1}) for MHC and MHCB, respectively, at 298 K. The magnitude of k_q estimated from the known value of τ_0 = 4.2 ± 0.1 ns (which was measured independently by exciting the protein solution at 295 nm[47]) is 1.77 and 0.63 (10^{14}, M^{-1} s^{-1}), respectively. This quantity is almost 3–4 orders of magnitude higher than the maximum possible value of k_q ($\approx 1 \times 10^{10}$ M^{-1} s^{-1}) for a purely diffusion-controlled (dynamic) quenching process, which suggests the formation of a ground state complex between HSA and the coumarin derivatives (static mechanism).

Characterizing the association of MHC and MHCB in the protein binding domain

The binding constant (K_b) of the investigated coumarins (ligand) with the protein and the number of binding sites (n) of the protein were determined from the fluorescence titration data using eqn (4) at different temperatures by considering (a) an equilibrium between the unbound and ligand-bound protein molecules and (b) the presence of similar but independent binding sites in the protein surface.[48]

$$\log\left[\frac{I_0 - I}{I}\right] = \log K_b + n\log[\text{ligand}] \quad (4)$$

Some of the representative plots where the data was fitted with the above equation to calculate the magnitudes of $\log K_b$ and n are shown in Fig. 7 and the ESI† (Fig. S5). The corresponding values estimated from the intercept and slope of the double-log analysis for both systems are presented in Table 3. The average number of binding sites for the coumarin derivatives is close to one, corresponding to the single binding site of HSA at subdomain IIA (Sudlow site I). However, the magnitude of n is higher for MHC in comparison with MHCB, suggesting the relatively stronger interaction of the former with HSA. This observation is consistent with relatively higher values of K_{SV} and K_b in MHC obtained from the fluorescence titration data and the complimentary results obtained from CD and molecular docking calculation (see below).

It is interesting to note that the binding constant values for the investigated coumarin derivatives with HSA are moderate and vary within the order of 10^7–10^5 M^{-1}. Since HSA plays a significant role as a carrier protein, drug binding with HSA is an active screening test to estimate therapeutic possibilities.[49] Similar studies are common even for other biological macromolecules such as DNA.[50] In general, the role of HSA is to shield bound drugs from oxidation and release them at specific targets to produce therapeutic effects. Therefore, compounds with higher affinity for HSA allow easier drug transport *in vivo*. However, as discussed before, the strong sequestration of cholinergic compounds with HSA reduces the active fraction of the drug to inhibit AChE activity, and therefore, is no longer considered to be potent for the treatment of AD. A subtle balance between these two requirements with moderate affinity to HSA, equivalent to that estimated for the investigated coumarin derivatives in the present study, seems to be suitable to optimize the efficiency of anti-cholinergic drugs *in vivo*.

Considering the enthalpy (ΔH^0) and entropy (ΔS^0) change to be independent of temperature, all the thermodynamic parameters and spontaneity (given by the free energy change, ΔG) of the ligand binding process were obtained from the following set of equations by performing the fluorescence titration experiment at different temperatures.

$$\log K_b = -\frac{\Delta H^0}{2.303R} \times \frac{1}{T} + \frac{\Delta S^0}{2.303R}; \quad \Delta G^0 = \Delta H^0 - T\Delta S^0 \quad (5)$$

Interestingly, the results given in Fig. 7c and d and in Table 3 indicate that the magnitude of K_{SV} and K_b decreases with an increase in temperature for both compounds, further

confirming the hypothesis of ground state complex formation (static mechanism) for fluorescence quenching discussed earlier. Nonetheless, the negative free energy change (ΔG^0) for both cases indicates the spontaneous binding process of these compounds to HSA. The type of non-covalent interactions responsible for the binding of organic molecules on the protein surface is often characterized by the sign and magnitude of thermodynamic entities such as ΔS^0 and ΔH^0.[51] A positive ΔS value is mostly indicative of a hydrophobic mechanism in drug–protein interaction. On the other hand, negative entropy and enthalpy changes indicate the importance of van der Waals force and hydrogen bond formation. From the results displayed in Table 3, can be inferred that the hydrophobic interaction plays the leading role in MHCB binding with has, whereas, van der Waals force and/or hydrogen bond formation becomes relevant in the case of MHC. The difference in predominant forces controlling the binding for both coumarin compounds with a similar structural motif is presumably the primary factor for the variation in their binding thermodynamics with has, as discussed above.

Identification of protein secondary structure: circular dichroism measurement

Circular dichroism (CD) is a powerful tool to investigate the change in the secondary structure of the proteins when they interact with small molecules. The CD spectra of HSA exhibited two negative bands in the UV region at 208 and 222 nm (contributed by π–π* and n–π* transfer of α-helical structure of protein, respectively). The results of CD were converted into mean residual ellipticity (MRE) using the following relation:

$$\mathrm{MRE} = \frac{\text{Observed CD (mdegree)}}{C_p n l} \qquad (6)$$

where C_p is the molar concentration of the protein, n is the number of amino acid residues and l is the path length. The α-helical contents of free and complexed protein were calculated from the mean MRE values at 208 nm (MRE_{208}) using eqn (7).[52]

$$\alpha\text{-Helix}\ (\%) = \frac{[\mathrm{MRE}_{208} - 4000]}{[33\,000 - 4000]} \times 100 \qquad (7)$$

where 4000 is the MRE of the form and random coil conformation cross and 33 000 is the MRE value of a pure helix at 208 nm. As shown in the CD spectra of HSA in the absence and presence of the coumarin compounds (Fig. 8), the intensity of the negative band increases without any shift in the band maximum and the calculated α-helix content of HSA increases when it is bound to MHC or MHCB. The increase in ellipticity suggests that on complexation, both coumarin compounds stabilize the secondary structure of HSA.[53,54] This extra stabilization may arise because the hydroxyl group present in MHC and MHCB can bind with the amino acid residues of HSA to stabilize the protein helix structure.[55] The relatively higher stabilization in the case of MHC (inset, Fig. 8) in comparison with that of MHCB is consistent with the stronger interaction of the former with HSA, as revealed in the fluorescence titration experiment discussed before.

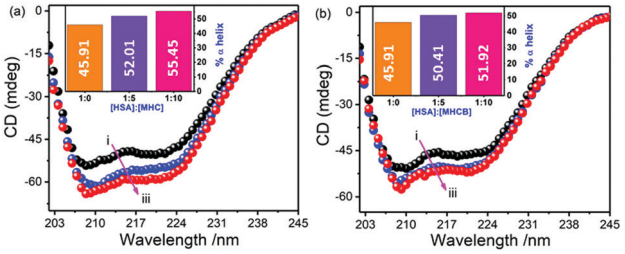

Fig. 8 Circular dichroism (CD) spectra of HSA in the presence of varying concentration of MHC (a) and MHCB (b). The protein–ligand concentration ratio increases along the arrow direction as 1 : 0 (i), 1 : 5 (ii) and 1 : 10 (iii). Inset shows the change in α-helix content of the protein calculated from the CD data in each case.

Characterizing the major forces for binding: molecular docking calculation

The blind docking results indicate that MHC sits in sub-domain IIA of drug site 1, whereas, MHCB binds to sub-domain IB of HSA. For targeted docking in MHC, the grid box was centred at 22.147 (x-centre), 32.155 (y-centre) and 36.265 (z-centre) with the corresponding size of 26, 28 and 28, respectively. On the other hand, a grid box value of 43.028, 31.207 and 17.906 for the x-, y-, and z-centres with a corresponding size of 28, 42 and 34, respectively, was set for MHCB in domain IB of HSA. From the best posed docked structure given in Fig. 9 and the corresponding energy parameters (Table 4), it was observed that MHC binds more favourably to the hydrophobic cavity in subdomain IIA with $\Delta G = -43.93$ kJ mol^{-1} (corresponding to $\log K = 7.69$) in comparison with MHCB ($\Delta G = -41.39$ kJ mol^{-1}, $\log K = 7.25$) in domain IB of HSA. The trend and values of the estimated

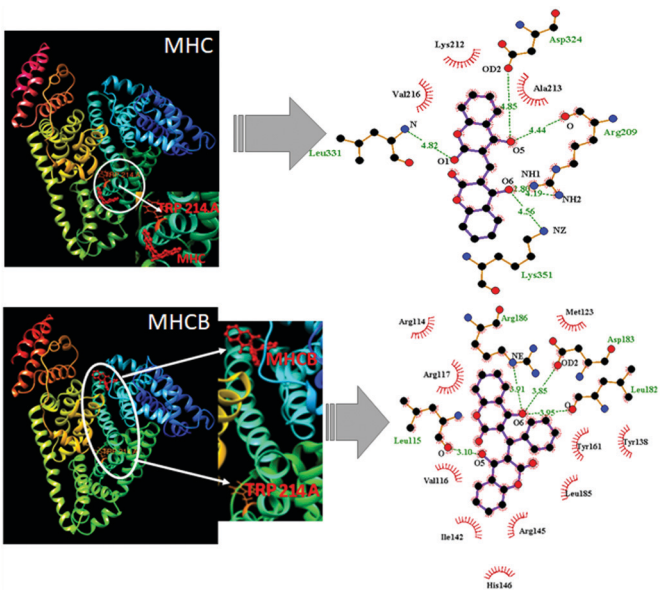

Fig. 9 Best docked poses of MHC and MHCB with HSA. The Ligplot images on the right-hand side depict the hydrogen bonding and hydrophobic interactions of the various residues of HSA with the compounds. Dotted lines represent hydrogen bonds, whereas, circular spikes show hydrophobic interactions.

Table 4 Molecular docking calculation results for the binding interaction of MHC (A) and MHCB (B) with HSA

		Hydrogen bonding interaction			
	Binding affinity/kJ mol^{-1}	n_{HB}	Residues involved	R_{HB}/Å	Hydrophobic interaction
A	−43.93	6	O2···N(Leu331)	4.82	Val216, Lys212, Ala213
			O5···OD2(Asp324)	4.85	
			O5···O(Arg209)	4.44	
			O6···NH1(Arg209)	2.80	
			O6···NH2(Arg209)	4.19	
			O6···NZ(Lys351)	4.56	
B	−41.39	4	O5···O(Leu115)	3.10	Arg114, Arg117, Val116, Ile142, His146,
			O6···NE(Arg186)	3.91	Arg145, Leu185, Tyr161, Tyr138, Met123
			O6···OD2(Asp183)	3.85	
			O6···O(Leu182)	3.95	

binding parameters match well with that obtained from the fluorescence experiments (ΔG = −41.37 kJ mol^{-1} for MHC and ΔG = −28.30 kJ mol^{-1} for MHCB). It should be noted here that molecular docking calculation gives a rough approximation of the binding sites. Further, since the larger protein structure is static and motion is allowed only to the smaller-sized drug molecules, extremely accurate determination of the energy parameters is not expected. Despite these inherent limitations, the calculated negative values of the affinities indicate spontaneous interaction in both coumarin derivatives investigated in this study and augurs well with the values obtained from the fluorescence experiments.

The amino acid residues Val216, Lys212, and Ala213 of site I are involved in the hydrophobic interaction to stabilize the complex formation for MHC. On the other hand, the ligand MHCB interacts hydrophobically with Arg114, Arg117, Val116, Ile142, His146, Arg145, Leu185, Tyr161, Tyr138, and Met123. Moreover, MHC forms a total of six hydrogen bonds (HB) with amino acid residues of HSA, of which one HB with Leu331 having a bond length (r_{HB}) of 4.82 Å, one with Asp324 (r_{HB} = 4.85 Å), three with Arg209 (r_{HB} = 4.44, 2.80 and 4.19 Å) and one with Lys351 (r_{HB} = 4.56 Å). Similarly, MHCB also forms four hydrogen bonds with other amino acid residues of HSA, namely Leu115 Arg186, Asp183 and Leu182 with r_{HB} = 3.10, 3.91, 3.85 and 3.95 Å, respectively. In both ligand–HSA complexes, it has been well observed that the hydroxyl oxygen of the ligand formed more hydrogen bonds with amino acid residues compared with the ketonic oxygen of the ligands to stabilize the complex formation.

Conclusions

The anticholinergic activity of the investigated coumarin compounds, MHC and MHCB, is comparable with some of the FDA approved drugs for the treatment of AD. However, the *in vitro* assessment of their AChE inhibition activity in the presence of the HSA matrix was found to decrease substantially as evidenced by the 12–14% increase in IC_{50} value for both systems, primarily due to the sequestration of the drugs in the HSA cavity through a combination of hydrophobic and hydrogen bonding (HB) interactions. Quantitative estimation of the HB effect was modeled with multiparametric regression of several spectroscopic responses based on the Kamlet–Taft and Catalán models. It was found that although about 20% of the solvatochromic response of the fluorescence yield was contributed through the solvent polarity and/or polarizability (π^*) term in MHC, it was almost insignificant for MHCB. Despite their similar structural architecture, the solvent HB donation acidity (α) and acceptance basicity (β) act differently for most of the spectral properties of the investigated systems. The modulation in fluorescence response in the hydrophobic cavity of cyclodextrin or at the protein binding domain in HSA is consistent with the solvatochromic analysis. Titration of the intrinsic tryptophan fluorescence in conjunction with molecular docking calculation reveals the strong sequestration tendency of HSA for both compounds and the results corroborate nicely with the relative decrease in AChE inhibition efficiency in the respective cases. These findings can help in understanding the binding and transport properties of coumarinyl compounds in human plasma at the molecular level, and therefore, can lead to the development of better AChE inhibitors.

Materials and methods

Synthesis and characterization MHC and MHCB

All commercially available chemicals and reagents used for the synthesis of the desired coumarin derivatives were purchased from Sigma Aldrich and Merck and were used without further purification. The synthesis of the compounds involved the earlier reported procedure[56] with slight modification and is given in Scheme 1. In brief, to a stirred solution of aldehyde 1 (2.0 mmol) and 4-hydroxy coumarin 2 (4.0 mmol) in 5 mL Millipore water, Ni nanoparticles (NPs) (25 mg mmol^{-1}) were added at room temperature. The reaction mixture was stirred at the same temperature for 3 h. After completion of the reaction (monitored by thin layer chromatography, TLC), the reaction mixture was filtered through a Buchner funnel, and washed with water. The residue was recrystallized from 5 mL ethanol to afford pure compounds **3a** and **3b**. The purity of the products was confirmed by infrared (IR), nuclear magnetic resonance (NMR) and mass spectroscopy (data given below). Melting points were determined in open capillary tubes and are uncorrected. IR spectra were recorded in potassium bromide (KBr) pellets on a PerkinElmer Spectrum 400 FTIR instrument, and the frequencies are expressed in cm^{-1}. ^{1}H-NMR and ^{13}C-NMR spectra were recorded on a Bruker Avance II-400 spectrometer in DMSO-d_6/$CDCl_3$

(chemical shifts in δ with TMS as an internal standard). Mass spectral data was obtained with a WATERS (ZQ-4000) mass spectrometer. All reactions were monitored by thin layer chromatography (TLC) using pre-coated aluminium sheets (silica gel 60 F_{254}, 0.2 mm thickness).

3,3′-Methylenebis(4-hydroxy-2*H*-chromen-2-one) (3a, MHC). White powder, mp: 218–220 °C; IR ν_{max} (KBr): 3380, 3045, 1640, 1615, 1579, 1293, 1084, 756 cm^{-1}; ^1H NMR ($CDCl_3$, 400 MHz): δ_H (ppm) 11.52 (s, 1H, OH), 11.24 (s, 1H, OH), 7.98–7.80 (m, 2H, Ar-H), 7.59–7.55 (m, 2H, Ar-H), 7.35–7.33 (m, 2H, Ar-H), 6.95–6.84 (m, 2H, Ar-H), 2.52 (s, 2H, CH_2); ^{13}C NMR (100 MHz, $CDCl_3$ + DMSO-d_6): δ_C (ppm) 164.49, 160.55, 151.88, 130.33, 128.12, 128.01, 127.34, 126.20, 124.01, 123.76, 115.89, 113.45, 23.06; MS (ES^+) calcd for $C_{19}H_{12}O_6$: 336.06, found *m*/*z* 337.09 $(M + H)^+$.

3,3′-(Phenylmethylene)bis(4-hydroxy-2*H*-chromen-2-one) (3b, MHCB). White crystal, mp: 228–230 °C; IR ν_{max} (KBr): 3399, 3070, 1659, 1618, 1569, 1282, 1093, 757 cm^{-1}; ^1H NMR ($CDCl_3$, 400 MHz): δ_H (ppm) 11.48 (s, 1H, OH), 11.26 (s, 1H, OH), 7.12–8.02 (m, 13H, Ar-H), 6.04 (s, 1H, 4H); ^{13}C NMR (100 MHz, $CDCl_3$): δ_C (ppm) 165.83, 164.62, 152.53, 152.29, 135.19, 132.88, 128.65, 126.89, 126.48, 124.92, 124.40, 116.83, 116.65, 105.63, 103.89, 36.17; MS (ES^+) calcd for $C_{25}H_{16}O_6$: 412.09, found *m*/*z* 413.12 $(M + H)^+$.

Solvents and reagents for spectral measurements

A series of ten organic solvents, all highest grade available with varying solvent parameters (listed in Table S1, ESI†) was procured from Sigma-Aldrich and used fresh to make 3–5 μM concentration of the probe necessary for spectroscopic measurements. Purified water, collected from an Elix 10 water purification system (Millipore India Pvt. Ltd) was used to make the aqueous solutions. Analytically pure β-cyclodextrin (β-CDx) and human serum albumin (fraction V, lyophilized powder form of HSA) were also used as received from Sigma-Aldrich. Analytically best grade available reagents were used for measuring the enzyme activity of AChE, the details of which are mentioned elsewhere.[25]

Instruments and data analysis

Estimation of the acetylcholinesterase (AChE) inhibition activity of the investigated coumarin compounds was done in a Synergy H1 hybrid meter plate reader instrument (BioTek) using 96-well plates following the protocol reported earlier.[25,37] A brief description of the adopted procedure and data handling techniques is also given in the ESI† (ST1). Cuvette-based UV-vis absorption and steady-state fluorescence emission/excitation spectra were collected in PerkinElmer Lambda25 and Hitachi F4500 spectrophotometers, respectively. All experiments were carried out at room temperature (298 ± 2 K) with 10 mm quartz cuvettes. For the fluorescence experiments, a 5 nm bandpass was used in both the emission/excitation side and all the spectra were corrected for photomultiplier response within the measured wavelength range. Each of the fluorescence spectra of both probes in heterogeneous media, taken as the average of three independent measurements, was further corrected for possible signal attenuation due to the presence of substances other than the fluorophore using the method described elsewhere.[57] Fluorescence quantum yields (ϕ_f) were calculated by comparing the total intensity under the whole fluorescence spectral range with that of a standard (quinine bisulfate in 0.5 M H_2SO_4 solution, $\phi_f^s = 0.546$[58]) following the protocol described earlier.[46] The relative experimental error in the measurement of ϕ_f was estimated to be ±10%.[59]

Time-resolved fluorescence decay measurements were performed in a fluorescence spectrometer (QM-40, PTI, USA) equipped with a TCSPC fluorescence lifetime detection unit (PM-3). The sample was excited by a 295 nm nano-LED supplied by PTI. The experimentally obtained decay traces were expressed as a sum of exponentials (eqn (8)) and fitted with the iterative deconvolution method based on the Levenberg–Marquardt algorithm[60] with reference to the instrument response function (IRF), collected at the excitation wavelength using a scattering solution. The success of the fitting model was checked by noting the reduced chi-square (χ^2) and Durbin–Watson (DW) parameter along with visual inspection of the residual distribution in the whole fitting range.

$$F(t) = \sum_i \alpha_i \exp\left(\frac{-t}{\tau_i}\right) \quad (8)$$

where α_i is the amplitude of the *i*th component associated with fluorescence lifetime τ_i such that $\Sigma\alpha_i = 1$. For non-exponential fitted functions, the average lifetime (τ_{av}) was expressed in terms of fractional contribution (f_i) of each decay time to the steady state intensity with the following equation.[46]

$$\tau_{av} = \sum_i f_i\tau_i = \frac{\sum_i \alpha_i\tau_i^2}{\sum_i \alpha_i\tau_i} \quad (9)$$

Further, estimation of the radiative (κ_r) and total non-radiative ($\Sigma\kappa_{nr}$) decay rate constants in each case was done with the known values of ϕ_f and τ_{av} using the following set of relations, and the values are given in the table.

$$\kappa^r = \frac{\phi_f}{\tau_{av}}; \quad \Sigma\kappa^{nr} = \frac{(1-\phi_f)}{\tau_{av}} \quad (10)$$

Variation in solvatochromic data was checked with the three-parameter-based Kamlet–Taft (KT) or four-parameter-based Catalán model. The detailed protocol for multiple regressions with the KT relation is given elsewhere.[32–34] Additionally, we also analyzed the spectroscopic properties with the four-parameter Catalán scale[31,35] with the intention to isolate the independent contribution from solvent polarizability (SP) and solvent dipolarity (SdP).

Molecular docking calculation

Molecular docking calculation was performed to disclose the binding site and identify several interactions involved between the amino acid residues of HSA and the guest to stabilize the HSA–ligand complex. For the molecular docking calculation, the 3D structure of HSA (PDB ID: 1AO6) was retrieved from the Protein Data Bank (www.rcsb.org). The structure was prepared for docking by the removal of all heteroatoms, including ions and water molecules, addition of polar hydrogen and assignment of Kollman charges. The coumarin compounds (MHC and MHCB) were modelled using ChemDraw and minimized using the MMF4

force field.[61] The docking studies were executed with the help of AutoDock Vina and AutoDock tools-1.5.6 (ADT)[62] and fashioned using Chimera[63] using the protocol of Lamarckian Genetic Algorithm (LGA).[64] The number of docking runs was set to 50. The conformational cluster analysis was done using the maximum RMS tolerance of 2.00 and the lowest energy conformer was chosen for sketching the docked poses.

Conflicts of interest

There are no conflicts to declare.

Acknowledgements

The authors acknowledge the support from the Dept. of Science & Technology (DST), Govt. of India to the Chemistry Department through FIST program (SR/FST/CSI-194/2008).

Notes and references

1 T. S. Reddy and A. R. Reddy, *Dyes Pigm.*, 2013, **96**, 525–534.
2 J. R. Hoult and M. Paya, *Gen. Pharmacol.*, 1996, **27**, 713–722.
3 E. C. Gaudino, S. Tagliapietra, K. Martina, G. Palmisano and G. Cravotto, *RSC Adv.*, 2016, **6**, 46394–46405.
4 S. Widmer, M. Dorrestijn, A. Camerlo, S. K. Urek, A. Lobnik, C. E. Housecroft, E. C. Constableb and L. J. Scherer, *Analyst*, 2014, **139**, 4335–4342.
5 F. J. Duarte, *Tunable Laser Optics*, New York, Elsevier-Academic, 2003.
6 K. P. Carter, A. M. Young and A. E. Palmer, *Chem. Rev.*, 2014, **114**, 4564–4601.
7 X. M. Peng, G. L. Damu and C. Zhou, *Curr. Pharm. Des.*, 2013, **19**, 3884–3930.
8 M. Mladenovic, N. Vukovic, N. Niciforovic, S. Sukdolak and S. Solujic, *Molecules*, 2009, **14**, 1495–1512.
9 A. S. Al-Ayed and N. Hamdi, *Molecules*, 2014, **19**, 911–924.
10 K. V. Sashidhara, A. Kumar, M. Kumar, J. Sarkar and S. Sinha, *Bioorg. Med. Chem. Lett.*, 2010, **20**, 7205–7211.
11 O. Pelkonen, H. Raunio, A. Rautio, M. Pasanen and M. A. Lang, *The Metabolism of Coumarin. Coumarins: Biology, Applications and Mode of Action*, Chichester, John Wiley & Sons, 1997, pp. 67–92.
12 J. I. Weitz, Blood Coagulation and Anticoagulant, Fibrinolytic, and Antiplatelet Drugs, in *Goodman & Gilman's: The Pharmacological Basis of Therapeutics*, 12th edn, 2011, ISBN: 978-0-07-175352-4.
13 R. D. Thornes, *Ir. Med. J.*, 1983, **76**, 225.
14 J. R. Casley-Smith, in *Coumarin in the Treatment of Lymphoedema and Other High-Protein Oedemas. Coumarins: Biology, Applications and Mode of Action*, ed. R. O'Kennedy and R. D. Thornes, John Wiley & Sons, Chichester, 1997, vol. 46, pp. 143–184.
15 R. M. Christie, K. M. Morgan and M. S. Islam, *Dyes Pigm.*, 2008, **76**, 741–747.
16 W. Lin, L. Yuan, J. Feng and X. Cao, *Eur. J. Org. Chem.*, 2008, 2689–2692.
17 J. Wang, X. Qian and J. Cui, *J. Org. Chem.*, 2006, **71**, 4308–4311.
18 M. T. Lee, C. K. Yen, W. P. Yang, H. H. Chen, C. H. Liao, C. H. Tsai and C. H. Chen, *Org. Lett.*, 2004, **6**, 1241–1244.
19 J. M. Hierrezuelo and C. C. Ruiz, *J. Phys. Chem. A*, 2012, **116**, 12476–12485.
20 S. Nad and H. Pal, *J. Phys. Chem. A*, 2003, **107**, 501–507.
21 M. Homocianu, A. Airinei and D. O. Dorohoi, *J. Adv. Res. Phys.*, 2011, **2**, 1–9.
22 Y. Yue, S. Zhao, Y. Sun, X. Yan, J. Liu and J. Zhang, *J. Lumin.*, 2017, **187**, 333–339.
23 A. Garg, D. M. Manidhar, M. Gokara, C. Malleda, C. S. Reddy and R. Subramanyam, *PLoS One*, 2013, **8**, e63805.
24 Y. Yue, Z. Wang, Z. Wang, Y. Zhang and J. Liu, *J. Mol. Struct.*, 2018, **1169**, 75–80.
25 P. Baruah, G. Basumatary, S. O. Yesylevskyy, K. Aguan, G. Bez and S. Mitra, *J. Biomol. Struct. Dyn.*, 2019, **37**, 1750–1765.
26 I. Matei, S. Ionescu and M. Hillebrand, Solute-solvent hydrogen bond formation in the excited state. Experimental and theoretical evidence, in *Hydrogen bonding and transfer in the excited state*, ed. K.-L. Han and G.-J. Zhao, John Wiley & Sons Ltd, Chichester, UK, 2010, ch. 4.
27 F. D. Lewis and W. Weigel, *J. Phys. Chem. A*, 2000, **104**, 8146–8153.
28 T. S. Singh, S. Mitra, A. K. Chandra, N. Tamai and S. Kar, *J. Photochem. Photobiol., A*, 2008, **197**, 295–305.
29 J. Zou, Q. Yu and Z. Shang, *J. Chem. Soc.*, 2001, **2**, 1439–1443.
30 M. J. Kamlet, J. M. Abboud, M. H. Abraham and R. W. Taft, *J. Org. Chem.*, 1983, **48**, 2877–2887.
31 J. Catalán, *J. Phys. Chem. B*, 2009, **113**, 5951–5960.
32 N. S. Moyon, A. K. Chandra and S. Mitra, *J. Phys. Chem. A*, 2010, **114**, 60–67.
33 N. S. Moyon, P. M. Gashnga, S. Phukan and S. Mitra, *Chem. Phys.*, 2013, **421**, 22–31.
34 N. S. Moyon and S. Mitra, *J. Phys. Chem. A*, 2011, **115**, 2456–2464.
35 M. A. Rohman, P. Baruah, S. O. Yesylevskyy and S. Mitra, *Chem. Phys.*, 2019, **517**, 67–79.
36 H. Dvir, I. Silman, M. Harel, T. L. Rosenberry and J. L. Sussman, *Chem. – Biol. Interact.*, 2010, **187**, 10–22.
37 P. Baruah, M. A. Rohman, S. O. Yesylevskyy and S. Mitra, *Bioimpacts*, 2019, **9**, 85–96.
38 P. Anand, B. Singh and N. Singh, *Bioorg. Med. Chem.*, 2012, **20**, 1175–1180.
39 M. M. Islam, A. B. Gurung, A. Bhatacharjee, K. Aguan and S. Mitra, *Chem. – Biol. Interact.*, 2016, **249**, 1–9.
40 M. A. Rohman, D. Sutradhar, S. Sangilipandi, K. Mohan Rao, A. K. Chandra and S. Mitra, *J. Photochem. Photobiol., A*, 2017, **341**, 115–126.
41 J. Kuchlyan, D. Banik, A. Roy, N. Kundu and N. Sarkar, *J. Phys. Chem. B*, 2014, **118**, 13946–13953.
42 S. Banerjee, S. Roy and B. Bagchi, *J. Phys. Chem. B*, 2010, **114**, 12875–12882.
43 S. Jacob and A. B. Nair, *Drug Dev. Res.*, 2018, **79**, 201–217.
44 G. Tiwari, R. Tiwari and A. K. Rai, *J. Pharm. BioAllied Sci.*, 2010, **2**, 72–79.
45 B. D. Wang, J. Hai, Z. C. Liu, Q. Wang, Z. Y. Yang and S. H. Sun, *Angew. Chem., Int. Ed.*, 2010, **49**, 4576–4579.

46 J. R. Lakowicz, *Principles of Fluorescence Spectroscopy*, Springer, Singapore, 2006.
47 M. A. Rohman, K. Saha and S. Mitra, *J. Biomol. Struct. Dyn.*, 2019, **37**, 4737–4746.
48 V. K. Sonu, M. M. Islam, M. A. Rohman and S. Mitra, *Colloids Surf., B*, 2016, **146**, 514–522.
49 Z. Sharif-Barfeh, S. Beigoli, S. Marouzi, A. S. Rad, A. Asoodeh and J. Chamani, *J. Solution Chem.*, 2017, **46**, 488–504.
50 A. A. Moosavi-Movahedi, A. R. Golchin, K. Nazari, J. Chamani, A. A. Saboury, S. Z. Bathaie and S. Tangestani-Nejad, *Thermochim. Acta*, 2004, **414**, 233–241.
51 P. D. Ross and S. Subramanian, *Biochemistry*, 1981, **20**, 3096–3102.
52 P. B. Kandagal, S. Ashoka, J. Seetharamappa, S. M. T. Shaikh, Y. Jadegoud and O. B. Ijare, *J. Pharm. Biomed. Anal.*, 2006, **41**, 393–399.
53 V. D. Porta, E. Bramanti, B. Campanella, M. R. Tiné and C. Duce, *RSC Adv.*, 2016, **6**, 72386–72398.
54 R. W. Woody, *Circular Dichroism and the Conformational Analysis of Biomolecules*, Plenum Press, New York, 1996, pp. 25–67.
55 J. N. Miller, *Proc. Anal. Div. Chem. Soc.*, 1979, **16**, 203–208.
56 D. Bhattacharjee, S. K. Sheet, S. Khatua, K. Biswas, S. Joshi and B. Myrboh, *Bioorg. Med. Chem.*, 2018, **26**, 5018–5028.
57 B. Valeur and M. N. Berberan-Santos, *Molecular fluorescence: principles and applications*, Wiley-VCH, 2012.
58 J. N. Demas and G. A. Crosby, *J. Phys. Chem.*, 1971, **75**, 991–1024.
59 S. Phukan, M. Saha, A. K. Pal, A. C. Bhasikuttan and S. Mitra, *J. Photochem. Photobiol., A*, 2015, **303**, 67–79.
60 P. R. Bevington, *Data Reduction and Error Analysis for the Physical Sciences*, McGraw-Hill, New York, 1969.
61 T. Halgren, *J. Comput. Chem.*, 1996, **17**, 490–519.
62 D. Seeliger and B. L. de Groot, *J. Comput.-Aided Mol. Des.*, 2010, **24**, 417–422.
63 E. F. Pettersen, T. D. Goddard, C. C. Huang, G. S. Couch, D. M. Greenblatt, E. C. Meng and T. E. Ferrin, *J. Comput. Chem.*, 2004, **25**, 1605–1612.
64 M. Fasano, S. Curry, E. Terreno, M. Galliano, G. Fanali, P. Narciso, S. Notari and P. Ascenzi, *IUBMB Life*, 2005, **57**, 787–796.